Journal of Environmental Chemical Engineering 11 (2023) 110806

Contents lists available at ScienceDirect

Journal of Environmental Chemical Engineering

journal homepage: www.elsevier.com/locate/jece

Hybrid multi-core shell magnetic nanoparticles for wet peroxide oxidation of paracetamol: Application in synthetic and real matrices

Adriano S. Silva [a,b,*], Fernanda F. Roman [a,b], Arnaldo V. Dias [a,b,c], Jose L. Diaz de Tuesta [d], Alexandre Narcizo [a,b], Ana Paula F. da Silva [a,b], Ihsan Çaha [e], Francis Leonard Deepak [e], Manuel Bañobre-López [e], Ana M.C. Ferrari [f], Helder T. Gomes [a,b,*]

[a] Centro de Investigação de Montanha (CIMO), Instituto Politécnico de Bragança, Campus de Santa Apolónia, 5300-253 Bragança, Portugal
[b] Laboratório Associado para a Sustentabilidade e Tecnologia em Regiões de Montanha (SusTEC), Instituto Politécnico de Bragança, Campus de Santa Apolónia, 5300-253 Bragança, Portugal
[c] Universidade Tecnológica Federal do Paraná (UTFPR), Campus Apucarana, 86812-460 Apucarana, Brazil
[d] Department of Chemical and Environmental Technology, ESCET, Rey Juan Carlos University, C/Tulipan s/n, 28933 Móstoles, Madrid, Spain
[e] Advanced (Magnetic) Theranostic Nanostructures Lab, International Iberian Nanotechnology Laboratory, Av. Mestre Jose Veiga s/n, 4715-330 Braga, Portugal
[f] Universidade Tecnológica Federal do Paraná (UTFPR), Campus Londrina, 86036-370 Londrina, Brazil

ARTICLE INFO

Editor: Despo Kassinos

Keywords:
Heterogeneous Fenton
Contaminants of emerging concern
Real wastewater
Advanced oxidation process
Micropollutants
Carbon-coated nanoparticle

ABSTRACT

Clean water availability is becoming a matter of global concern in the last decades. The responsible entities for wastewater treatment do not have the proper facilities to deal with a wide range of pollutants. Special attention should be given to emerging contaminants, whose presence in water bodies may cause adverse effects on the aquatic ecosystem and human health. Most studies in the literature do not consider the development of their solution in real matrices, which can hinder the applicability of the explored alternative in the real scenario. Therefore, in this work, we demonstrate the applicability of hybrid magnetic nanoparticles for removing paracetamol (PCM) from simulated and real matrices by catalytic wet peroxide oxidation (CWPO). To achieve carbon coating, the nanoparticles were prepared *via* the traditional route (resorcinol/formaldehyde, CoFe@CRF). A new methodology was also considered for synthesizing thin-layered carbon-coated magnetic nanoparticles (phloroglucinol/glyoxalic acid, CoFe@C_{PG}). TEM images revealed a multi-core shell structure formation, with an average carbon layer size of 7.8 ± 0.5 and 3.2 ± 0.3 nm for resorcinol/formaldehyde and phloroglucinol/glyoxalic acid methodology, respectively. Screening the materials' activity for PCM oxidation by CWPO revealed that the nanoparticle prepared by phloroglucinol/glyoxalic acid methodology has higher performance for the degradation of PCM, achieving 63.5% mineralization after 24 h of reaction, with similar results for more complex matrices. Iron leaching measured at the end of all reactions has proven that the carbon layer protects the core against leaching.

1. Introduction

Unplanned city growth is currently pressing the systems dealing with solid and liquid waste management [1,2]. The contamination of water bodies with a wide range of pollutants is being reported worldwide due to the increased utilization of personal care products, pharmaceuticals, pesticides, and natural and synthetic hormones [3–6]. These are known as contaminants of emerging concern (CECs), and commonly, their presence in water bodies is not monitored [3]. The ubiquitous presence and disturbance of ecological stability are the main factors leading to increased awareness of the scientific community of the dangers of CECs presence in water bodies [7–12].

Since the late 60 s, scholars have demonstrated that wastewater treatment plant facilities cannot properly remove a wide range of CECs. The lack of proper treatment at this stage is a major environmental problem, considering that this leads to the accumulation of CECs in water bodies, threatening water ecosystems and human health [13,14]. Pharmaceuticals have been recognized as increasingly troublesome

* Corresponding authors at: Centro de Investigação de Montanha (CIMO), Instituto Politécnico de Bragança, Campus de Santa Apolónia, 5300-253 Bragança, Portugal.
E-mail addresses: adriano.santossilva@ipb.pt (A.S. Silva), htgomes@ipb.pt (H.T. Gomes).

https://doi.org/10.1016/j.jece.2023.110806
Received 29 May 2023; Received in revised form 17 July 2023; Accepted 18 August 2023
Available online 22 August 2023
2213-3437/© 2023 The Author(s). Published by Elsevier Ltd. This is an open access article under the CC BY license (http://creativecommons.org/licenses/by/4.0/).

contaminants, with many studies reporting their presence in rivers, lakes, and other water bodies [15,16]. This class of compounds is used for several purposes, such as nutrition, prevention, treatments and diagnostics. The most common path for discharging pharmaceutical compounds in water bodies is improper human waste disposal of unwanted medication and pharmaceuticals in agriculture [17,18].

Several options for the treatment of CECs are reported in the literature, such as adsorption [19], forward osmosis [20], nanofiltration [21], ultrafiltration [22], biodegradation [23], and advanced oxidation processes [24–27]. Advanced oxidation processes (AOPs) emerge as a group of technologies based on the formation of highly oxidizing species, such as hydroxyl radicals, hydroperoxyl radicals, superoxide radicals, and sulfate radicals, for the degradation of organic pollutants [28,29]. There are several AOPs reported in the literature, such as photochemical [30], radiation-induced [31], cavitation [32], and electrochemical oxidation [33]. Despite the many approaches developed towards AOPs, the major and recognized limitation is the large-scale cost of implementing the treatments [34].

Among the AOPs, catalytic wet peroxide oxidation (CWPO) is typically conducted with a solid material as a catalyst [35]. A wide range of materials has been reported in the literature for removing organic pollutants, such as clay-based [24], carbon-based [36], waste-based [37], and magnetic catalysts [38]. The typical catalyst for this purpose comprises an active phase, such as transition metals (Fe, Ni, Co) supported on a highly stable material. The activity of the pioneer metal-based materials comes from the metal phase. Still, the operating conditions during oxidation reactions might lead to the release of metallic particles into the liquid media if the catalyst is not stable enough, resulting in pollution and activity loss [39]. Evolutions in research towards solving the iron leaching issue have led to using non-metal catalysts, for example, carbonaceous materials for CWPO, which returned promising results for mineralizing organic pollutants [40]. The activity in these catalysts comes from the redox properties of carbon-based materials, allowing the catalyst to interact with H_2O_2 to form hydroxyl radicals [41]. In general, most works dealing with CWPO explore the degradation of model pollutants in distilled or pure water (synthetic wastewater), which is far from real scenarios. Real matrices present several challenges to implementing CWPO technology, such as the presence of radical scavengers that may result in parasitic reactions affecting the amount of hydroxyl radicals available for pollutant degradation [42]. In addition, many pre-treatment and primary treatments (*e.g.,* coagulation-flocculation) cannot completely remove hydroxyl radical scavengers [26].

In most recent approaches, magnetic metal nanoparticles were carbon coated, showing a promising application in the catalytic degradation of pollutants [43]. Carbon-coated nanocatalysts have revealed a synergistic effect between the carbon layer and the inorganic core, typically composed of an active phase. This may be ascribed to the capacity of the carbon layer and the metal core to interact with the oxidant and contribute to hydroxyl radical formation. In addition, the carbon coating protects the metal core against metal leaching. Most works dealing with carbon-coated magnetic nanoparticles explore the utilization of phenol or resorcinol/formaldehyde (RF) phenolic resin for the coating procedure [44–46]. Despite the interesting approach and results with RF carbon-coated nanocatalyst, RF resin formulation is hazardous due to the utilization of carcinogenic reactants (*i.e.,* formaldehyde) [47]. In this regard, there are scarce studies dealing with novel carbon coating methods for metal nanoparticles to develop efficient catalysts for advanced oxidation processes. In this work, we propose an alternative route for coating particles with a carbon shell using a phloroglucinol/glyoxylic acid (PG) resin, which is less hazardous than traditional RF methodology [48]. Similarly, most works explore architectures such as the traditional core-shell [38] or the yolk-shell [45] structure. In both cases, the authors do not discuss the coating effect on the magnetic properties of their nanomaterial, which is a desired feature to be maintained after coating. In contrast, carbon-coated multi-core shell magnetic nanoparticles (MCSNPs) are known to preserve the magnetic characteristics after the coating procedure [49], and, as far as we are aware, there are no studies in the literature considering the utilization of MCSNPs for advanced oxidation processes, especially considering novel coating procedures.

The present study focus on developing efficient hybrid multi-core shell magnetic nanocatalysts for removing a micropollutant by CWPO. Two methodologies were considered for synthesizing hybrid materials; one previously reported in the literature (resorcinol-formaldehyde, RF) [50], allowing the formation of a carbon layer around the core, and an innovative methodology (phloroglucinol-glyoxal acid, PG), allowing to obtain a thin carbon layer around the core. Both the core and the carbon-coated nanomaterials were evaluated as catalysts for paracetamol (PCM) mineralization, chosen as a model pharmaceutical pollutant by CWPO. The screening of the nanocatalysts was carried out in a matrix comprised of ultrapure water and pollutant. The stability of the best catalyst was further studied in ultrapure water matrices, maintaining a similar profile of PCM removal for up to 3 cycles. Finally, the best nanocatalyst was further used to remove PCM in three more complex matrices: bottled water, hospital wastewater, and river water.

2. Methodology

2.1. Reagents

The reagents used in this study are described in Text S1 in the SI.

2.2. Multi-core shell magnetic nanoparticles (MCSNPs) synthesis

The procedure used to achieve the desired multi-core shell architecture is based on a step-by-step methodology comprised of 4 phases: (a) synthesis of the magnetic core, (b) resin coating, (c) annealing, and (d) etching. The coating procedures considered in this work to achieve the multi-core shell architecture have two purposes: use a new methodology based on the employment of glyoxal and phloroglucinol resin for the development of thin carbon coating and compare the new methodology with the more traditional formaldehyde and phenol resin [50]. The general procedure adopted is illustrated in Fig. S1.

The magnetic core was prepared following a sol-gel methodology described elsewhere [45]. The detailed synthesis procedure can be seen in Text S2 in the SI.

Two methodologies were carried out for coating the particles: a traditional resorcinol-formaldehyde (RF) route and an innovative route considering phloroglucinol-glyoxal acid (PG). In brief, for the traditional methodology, 0.25 g of the magnetic core is suspended in 50 mL of distilled water with the aid of an ultrasonic bath. The suspension is then transferred to a two-necked round bottom flask previously loaded with 0.12 mL of ammonia reagent and 0.1 g of resorcinol. This mixture will remain stirring at 30 °C for 1 h to ensure proper dispersion of reactants. After this period, 0.21 mL of TEOS and 0.15 mL of formaldehyde are poured into the mixture, so the condensation reaction of TEOS and polymerization reaction of resorcinol and formaldehyde (RF) can start. Once the reaction starts, temperature and stirring are kept the same for 6 h, when the temperature is raised to 80 °C, remaining at this temperature for another 8 h. Once finished, the final solid is recovered from the mixture and washed several times with distilled water until rinsing waters reach neutral pH. The washing process is performed with the aid of a neodymium magnet, which is enough to recover the magnetic nanoparticles from liquid media. The final nanomaterial was named CoFe@R_{RF}.

For the second methodology followed to coat the core, phloroglucinol and glyoxal were used instead of resorcinol and formaldehyde. In addition, Pluronic ® F-127 was also added to develop the porosity of the thin carbon layer. Pluronic ® F-127 was previously loaded in the two-necked round bottom flask along with other reactants. The reactants were chosen based on studies reporting the possibility of

achieving carbonization of the phloroglucinol/glyoxalic acid resin [51]. The final nanomaterial was washed until rinsing waters reached neutral pH, dried, and labeled as CoFe@R_{PG}.

CoFe@R_{RF} and CoFe@R_{PG} coated nanoparticles were annealed in an inert atmosphere in a tubular furnace (ROS 50/250/12, Thermoconcept) following the heat treatment illustrated in Fig. S2, resulting in CoFe@-SiO_2. C_{RF} and CoFe@SiO_2. C_{PG}, respectively. Finally, the carbon-coated nanoparticles underwent an etching process by stirring them in a 10 M NaOH solution for 16 h at room temperature to remove the silica content. The final nanoparticles were washed until rinsing waters reached neutral pH and labeled as CoFe@C_{PG} and CoFe@C_{RF} (product of CoFe@SiO_2. C_{PG} and CoFe@SiO_2. C_{RF}, respectively).

2.3. Characterization techniques

The MCSNPs were characterized throughout the synthesis procedure to identify the chemical path during the production of the desired nanocatalysts, as described in other studies [52]. The samples were analyzed by transmission electron microscopy (TEM), X-ray diffraction (XRD), Fourier-transform infrared spectroscopy (FT-IR), thermogravimetric analysis (TGA), and magnetometer. Textural properties were determined upon analysis of N_2 isotherms. For a more detailed description of the characterization techniques and calculation methods, please consult Text S3 and Table S1.

2.4. Aqueous-phase oxidation runs

The procedure considered for the liquid-phase oxidation runs is well described in previous works. For further information, please consult Text S4, Fig. S3, and Eq. (S1-5) in SI.

3. Results and discussion

3.1. Morphology and textural properties of nanomaterials

The TEM images recorded from samples CoFe, CoFe@C_{RF}, and CoFe@C_{PG} are shown in Fig. 1(a, b, c). The images revealed the successful synthesis of nanoparticles for the bare core, with an average size of 45.5 ± 8.1 nm. Energy-Dispersive X-Ray Spectroscopy (EDS) images of the CoFe sample in Fig. S4 confirm the presence of cobalt and iron on the sample, indicating the formation of cobalt ferrite structures. Furthermore, Fig. S4(b) reveals the presence of a region (upper part of the image) with a predominance of iron-only phase, which is probably related to the presence of hematite in the sample, also observed by XRD results which will be discussed in Section 3.4. Previous works have reported cobalt ferrite nanoparticles sizes in the range of 34.7–69.5 nm, depending on the method considered to prepare the nanoparticles [53]. Another work has reported achieving smaller cobalt ferrite nanoparticles, with particle size in the range of 7–28 nm [54]. However, their sample had about 29% mass loss in TGA, indicating a high amount of impurities due to inadequate heat treatment. For the CoFe sample synthesized in this work, the higher size found for the sample is related to the heat treatment performed to remove impurities, which increases particle size due to sintering [55].

The formation of a multi-core shell structure for CoFe@C_{RF} and CoFe@C_{PG} is confirmed by TEM images shown in Fig. 1(b) and (c), respectively. The carbon layers around the multi-core shell have a thickness of 7.8 ± 0.5 nm for CoFe@C_{RF} and 3.2 ± 0.3 nm for CoFe@C_{PG} samples. The different thickness is related to the different methodologies used to obtain the desired architecture. Previous studies dealing with RF methodology to prepare carbon-coated magnetic nanoparticles claimed to achieve a yolk-shell structure, which makes it difficult to compare the thickness of the shell obtained in this study. To the best of our knowledge, no other works report similar carbon coating to the material CoFe@C_{PG} and thus, no comparisons with previously reported results can be made. EDS images obtained for CoFe@C_{RF} and

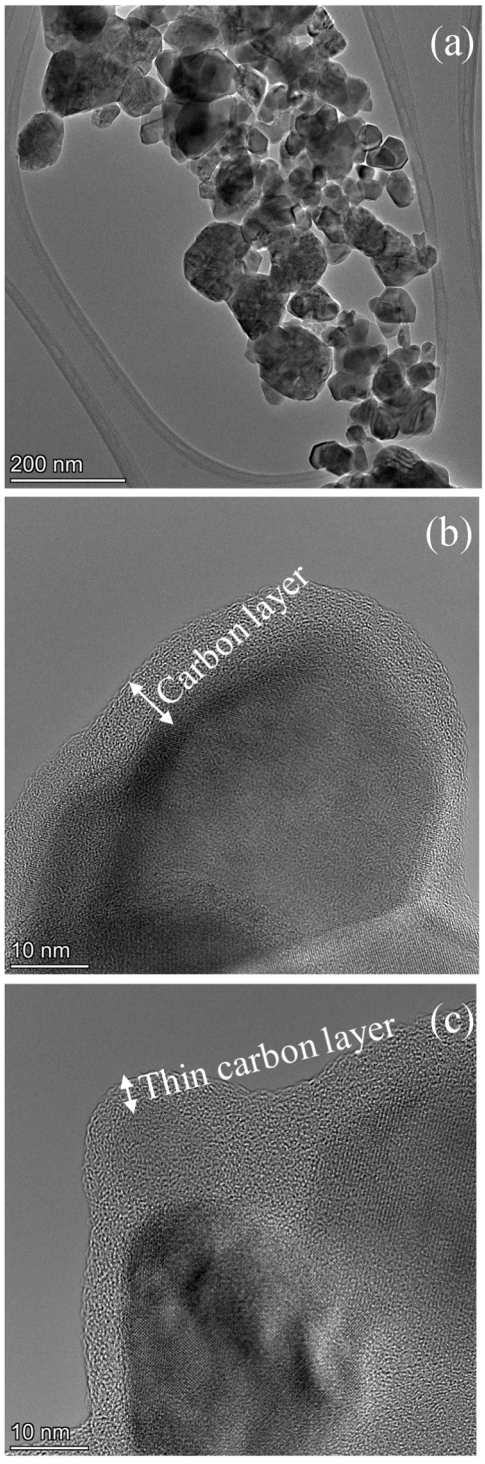

Fig. 1. TEM images of (a) CoFe, (b) CoFe@C_{RF}, (c) CoFe@C_{PG} samples.

CoFe@C_{PG} samples shown in Figs. S5 and S6, respectively, also confirmed the formation of the carbon layer. Additionally, the images revealed no presence of silica in the final multi-core shell nanoparticles, which indicates the successful silica removal in the etching process.

The N_2 adsorption isotherms of CoFe, CoFe@SiO_2. C_{RF}, CoFe@SiO_2. C_{PG}, CoFe@C_{RF}, and CoFe@C_{PG} are depicted in Fig. S7, and the textural properties obtained are outlined in Table S2. It can be seen from the figure that all nanomaterials show typical type IV isotherms with type H2 hysteresis, according to the classification established by IUPAC. This type of isotherm is given by mesoporous materials in which the

adsorbent-adsorptive interactions and the interactions between the molecules in the condensed state determine the adsorption behavior. The BET surface area for the materials presents a similar behavior for both synthesis routes, where the surface area increases with each step. The correlation coefficient obtained for each sample is displayed in Table S2. For instance, the surface areas for annealed samples CoFe@SiO_2. C_{RF} (43 m^2 g^{-1}) and CoFe@SiO_2. C_{PG} (16 m^2 g^{-1}) increased by 377% and 78%, respectively, compared to the bare core (9 m^2 g^{-1}). The nanomaterials obtained after the etching process (CoFe@C_{RF} and CoFe@C_{PG}) resulted in an increase in surface area of 533% and 144% (57 and 22 m^2 g^{-1}, respectively) compared to the bare core. Previous studies dealing with carbon-coated magnetic nanoparticles reported higher surface areas than reported in this study, in the range of 200–300 m^2 g^{-1} [43,46]. However, the step-by-step characterization reported here was not performed, making it more difficult to elucidate why a higher surface area was obtained. Nevertheless, the low surface area does not hinder the application of the nanoparticles as catalysts for CWPO purposes, since other studies already reported catalysts with smaller surface areas (S_{BET} ~ 13 – 26 m^2 g^{-1}) achieving high catalytic activity [56]. Most importantly, the material prepared for this application rather needs to possess active sites able to interact with H_2O_2 reactant to form hydroxyl radicals with good electron transfer properties (*i.e.,* carbon materials [57]) or the presence of transition metals (*i.e.,* iron and cobalt [56]).

3.2. Thermal stability of each nanomaterial during the synthesis procedure

TGA of each nanomaterial obtained during the experimental procedure (as presented in Fig. 2) and DTG under air atmosphere were used to study the formation of the desired carbon coating in both methodologies. The results are depicted in Fig. 2(a) and (b). The low mass loss observed for the bare core (CoFe sample) demonstrates the high purity of the inorganic material, with a mass loss of around 0.6% being obtained. The high inorganic content of the sample agrees with the literature, confirming the sol-gel potential for the synthesis of iron-based magnetic nanoparticles [58]. The resin-coated materials (CoFe@R_{RF} and CoFe@R_{PG}) are mainly comprised of a polymeric resin based on TEOS, phenolic compounds, and aldehyde. Both materials presented the highest mass loss compared to other samples, with 7.7% and 4.3% (at *ca.* 500 °C) for CoFe@R_{RF} and CoFe@R_{PG}, respectively. Following the polymerization and condensation reactions expected during the coating procedure, the thermal decomposition of the phenolic resin with a three-dimensional cross-linked inorganic network structure is responsible for the mass loss observed. The resin's structure is based on covalent O-bonds between the organic and inorganic (Si) phases. The peaks observed in DTG analysis, shown in Fig. 2(c) and (d), confirm the thermal decomposition of OH bonds from silanol and the organic content from the phenolic hybrid resins (200–400 °C). The difference in the mass loss for resin-coated samples is related to the formation of a thinner carbon layer for CoFe@R_{PG} compared to CoFe@R_{RF}, resulting in lower organic content.

The polymeric resin gives place to SiO_2 and graphitic shell after the annealing under N_2 atmosphere. The inorganic coating (Si) is present in higher amounts around the core, resulting from the electrochemical interaction between ammonium ions and the magnetic core, acting as directing agent for the condensation of TEOS around the core. The lower mass loss observed for both annealed samples of 2.8% (at *ca.* 310 °C) and 3.9% (at *ca.* 400 °C) for CoFe@SiO_2. C_{RF} and CoFe@SiO_2. C_{PG} is related to the removal of organic byproducts during thermal treatment. On the other hand, the presence of Si-O bonds is confirmed by the peak observed in the range 300–400 °C. At last, the lowest mass loss (apart from the core) was observed for final samples CoFe@C_{RF} and CoFe@C_{PG} due to the removal of silica in the etching. According to thermogravimetric results, the carbon content in the samples is around 1.8% and 0.8% for CoFe@C_{RF} and CoFe@C_{PG}. The carbon content observed for CoFe@C_{RF} is in agreement with the previously reported values obtained using the same methodology, with values below 5% [50]. As far as we know, no other work reports a similar carbon coating to the one shown here using a PG resin. The difference in carbon content in RF and PG methodologies is ascribed to the thickness of the carbon layer obtained for each methodology, with that obtained by PG resin to be much

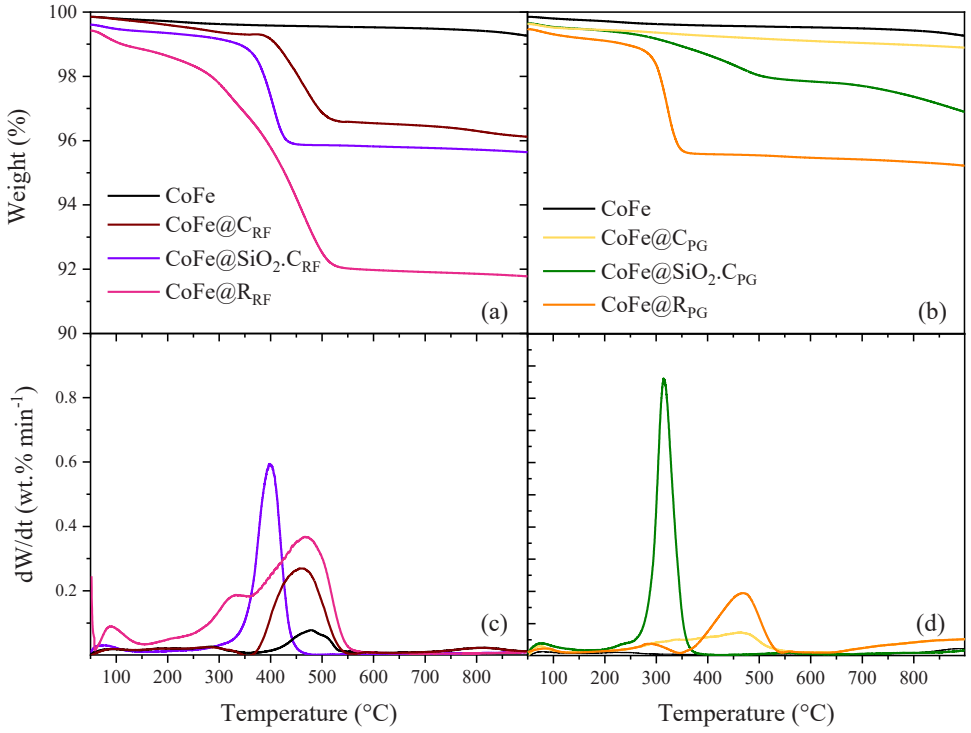

Fig. 2. Air-atmosphere TGA results of multi-core shell nanoparticles prepared with (a) RF and (b) PG resins; and DTG results for (c) RF and (d) PG coating methods.

thinner than that of the RF resin, as previously observed with TEM analysis.

3.3. Surface chemistry of the nanocatalysts

Chemical bond identification with FT-IR spectra reveals chemical modifications that are key steps for achieving the desired architecture in the final nanoparticles. The results obtained for FT-IR of CoFe, CoFe@SiO_2. C_{RF}, CoFe@SiO_2. C_{PG}, CoFe@C_{RF}, and CoFe@C_{PG} are shown in Fig. 3. Two main bands were observed at 496 and 560 cm^{-1} in Fig. 3(a), for the 3 materials prepared with PG resin, and at 464 and 556 cm^{-1} in Fig. 3(b), for the three materials prepared with RF resin. The bands between 460 and 500 cm^{-1} are attributed to the stretching vibration of octahedral sites of the Co-O bond, while the bands observed at a wavenumber around 560 cm^{-1} are attributed to the tetrahedral sites of the Fe-O bond. These results confirm the chemical bonds between cobalt oxides and iron oxides, indicating the presence of cobalt ferrite.

Strong and wide absorption bands around 1060 and 1089 cm^{-1} were also observed for CoFe@SiO_2. C_{RF}, CoFe@SiO_2. C_{PG}, CoFe@R_{RF} and CoFe@R_{PG} samples, which are attributable to Si-O-Si stretching vibrations, while the absorption bands around 800 and 960 cm^{-1} are assigned to Si-O symmetric stretching vibrations. Moreover, the band observed at 1618 cm^{-1} for the nanomaterials prepared by the traditional methodology (RF) is attributed to the bending vibration of H-O-H molecules and associated with water. For the final materials CoFe@C_{RF} and CoFe@C_{PG}, no signal related to Si-O-Si bonds was observed, evidencing the efficiency in removing SiO_2 by NaOH (10 mol L^{-1}) etching process for both coating methodologies.

3.4. Crystalline phase identification and magnetic properties

The bare core and final carbon-coated nanoparticles were analyzed by X-ray diffraction (XRD) to determine the crystalline phase composition and the effect of carbon coating on the core. The results obtained in this characterization were further processed in the software HighScore Plus to confirm the composition of the materials and acquire precise information further used to determine crystallite dimensions with the mathematical models proposed (core only). Fig. 4 displays the results acquired for all nanomaterials, and Fig. S8 illustrates the X-ray diffractograms for pure cobalt ferrite ($CoFe_2O_4$) and hematite (Fe_2O_3) (reference cards) from Crystallography Open Database (COD). The bare core composition was found to be a mixture of cobalt ferrite and hematite based on reference cards 96–153–3164 and 96–901–5965, respectively. Other works also reported the presence of iron phases as a byproduct in cobalt ferrite prepared by the sol-gel method [59], [60]. The presence of such a phase is related to the partial oxidation of iron from the Fe^{2+} state to the Fe^{3+}, overcoming parallel reactions that lead to the formation of hematite, maghemite, or even magnetite in some cases. Despite the identification of the hematite phase, resultant from iron that did not form cobalt ferrite, no other cobalt phase, rather than cobalt ferrite, was identified in this analysis (from possibly non-reacted Co ions).

Nevertheless, the semi-quantitative analysis performed with the aid of the HighScore Plus software revealed that the bare core sample is comprised of 95% cobalt ferrite and 5% hematite, which reveals a majority composition of the desired magnetic phase. The phase composition of carbon coated samples identified only cobalt ferrite, which is a direct consequence of the washing method used during the preparation of the nanoparticles. As described in the methodology, the washing step is performed with a strong neodymium magnet to recover the nanoparticles, which enables the removal of non-magnetic specimens from the sample. The carbon layer formed around the core in both methodologies does not influence the crystalline composition for traditional coating, as already reported in previous work [50]. Graphite card from COD (9011577) was also considered for the analysis, but the software was not able to identify the presence of such carbon conformation in this material, probably due to the small carbon content in the samples (< 4 wt%).

Additionally, the thin carbon coating does not affect the crystalline composition of the sample as well. Due to the hybrid composition of coated nanoparticles, the semi-quantitative analysis to determine the percentage and crystallite size determination by mathematical methods cannot be performed with XRD results since this could compromise the trustability of the reported values. For the bare core, the crystallite size

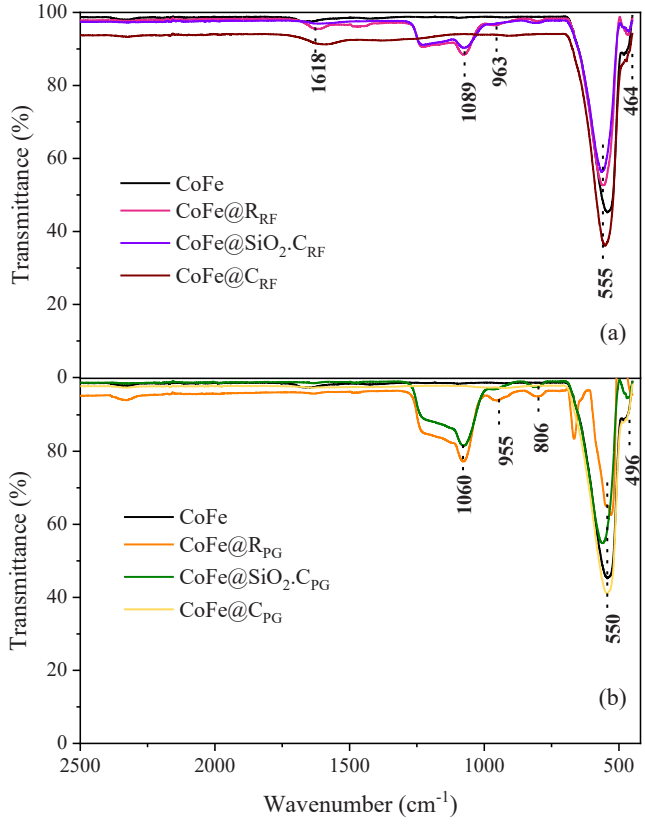

Fig. 3. FT-IR results for nanomaterials prepared with (a) resorcinol/formaldehyde and (b) phloroglucinol/glyoxalic acid resins.

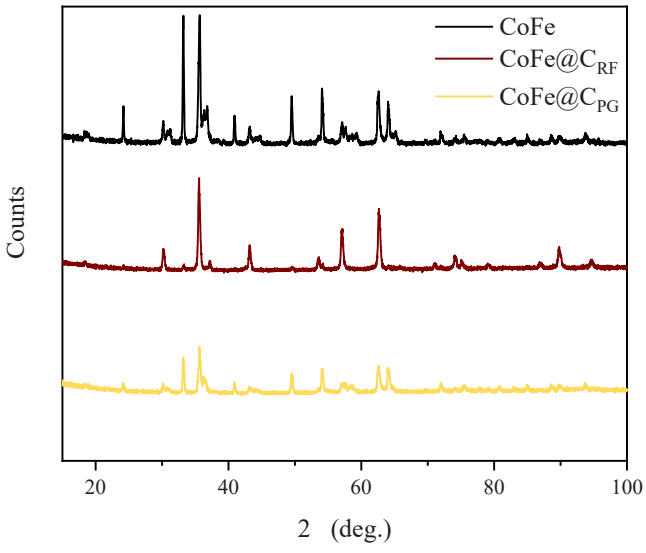

Fig. 4. X-Ray diffractogram for bare core and carbon-coated multi-core magnetic nanoparticles.

calculated with the mathematical methods returned 34.6 nm for Scherrer, 48.6 nm for Williamson-Hall, 43 nm for the Halder Wagner, and 56 nm for the Size-Strain plot method. The methods achieved about 24%, 7%, 5% and 23% error compared to TEM images, with the Halder-Wagner method allowing estimating a result closer to that observed by TEM images. Other studies have also reported Halder-Wagner as the method with higher accuracy for determining particle size using XRD data [50]. It is important to highlight that the comparison performed here is valid because the CoFe sample is a nanomaterial comprised of single crystallites.

The magnetization curve obtained for the bare core is shown in Fig. S9(a), along with the magnified region (−1.5 to 1.5 kOe) in Fig. S9 (b). The results reveal a saturation magnetization of around 67 emu g^{-1}, with a coercivity of 1.1 kOe and magnetic remanence value of 28.5 emu g^{-1}. The values found here are in agreement with the literature, with reported values between 33.8 and 87 emu g^{-1} [61] for saturation magnetization, values as high as 1.6 [61], 1.9 [62], and 1.4 [63] kOe for coercivity and 29.2 emu g^{-1} [62] for remanence. The values found for the bare core, along with the hysteresis loop, confirmed the ferrimagnetic characteristic of the sample [64]. The result obtained for the zero-field-cooling (ZFC) and field-cooling (FC) curves (Fig. S10) reveals no interception, indicating that the blocking temperature is above 300 K. The high blocking temperature obtained here indicates that magnetic core size is above the single-to-multidomain limit (6–7 nm), confirming the ferrimagnetic behavior of the sample [46].

3.5. Catalytic wet peroxide oxidation of paracetamol: catalyst screening

Fig. 5 illustrates the PCM and H_2O_2 concentration profiles obtained in the CWPO of PCM using the bare core (CoFe) and multi-core shell magnetic nanocatalysts. Compared to the non-catalytic run (X_{H2O2} = 10% and X_{PCM} = 13%), all nanoparticles have demonstrated catalytic activity towards the decomposition of H_2O_2 and abatement of PCM (complete removal after 24 h of reaction, regardless of the nanocatalyst). Thermal decomposition is responsible for the H_2O_2 degradation observed in the non-catalytic run performed at 80 °C. This amount of decomposed H_2O_2 was sufficient to promote the degradation of 13% of the pollutant's initial concentration in the system.

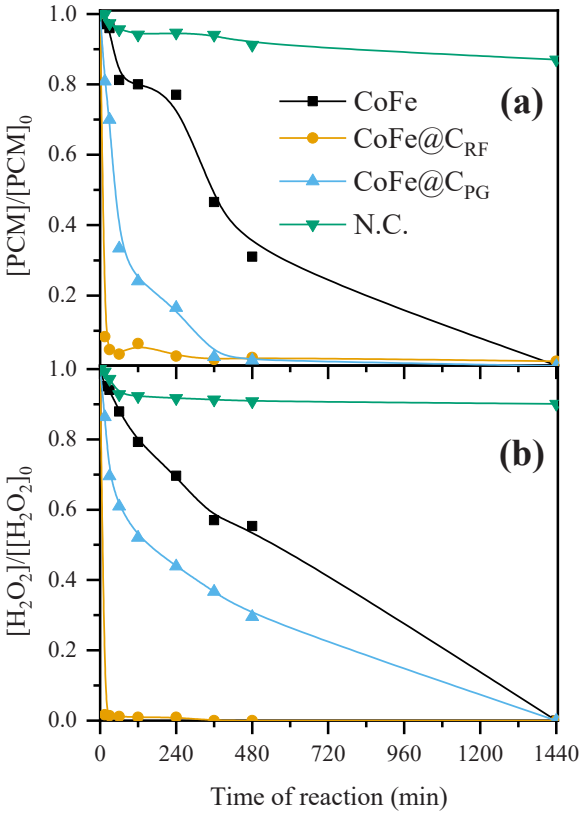

Fig. 5. Normalized concentration of (a) PCM and (b) H_2O_2 upon reaction time during CWPO experiences. Operating conditions: $[PCM]_0$ = 100 mg L^{-1}, $[H_2O_2]_0$ = 474 mg L^{-1}, [catalyst] = 2.5 g L^{-1}, pH_0 = 3.5, T = 80 °C.

Fig. 5(a) shows the PCM abatement. In the presence of CoFe@C_{RF} catalyst, PCM was rapidly abated since more than 90% of PCM had already been degraded after only 15 min of reaction. Similarly, the CoFe@C_{PG} catalyst produced a fast abatement of PCM, with almost 90% of the PCM being removed after 4 h of reaction. On the other hand, the uncoated nanocatalyst (CoFe bare core) led to a much slower removal of PCM, only achieving comparable results (> 90% of PCM removal) after 24 h of reaction. It should be noted that carbon layers and metallic phases simultaneously present in materials have a synergistic effect. Regardless of the preparation technique, more activity was shown for hybrid materials than for the pure core (CoFe bare cores). Both the metal phase and the carbon layer display electron-donor properties. Thus, a hybrid material containing both phases improves the electron transfer compared to a pure core. Electron transfer is the required condition to promote the degradation of H_2O_2, leading to the formation of hydroxyl radicals and, ultimately, to the removal of the pollutant from the system [65], and both metallic phases, such as iron and cobalt, and carbon layers allow for that electron transfer. Additionally, the more hydrophobic properties and larger surface area due to the carbon layer increase the adsorptive interactions between the pollutant and the catalyst's surface [43]. Finally, leaching protection allows the catalyst's useful life to be extended. Similar findings have been reported in the literature, where hybrid materials with metal and carbon phases showed greater activity than pure metal phases [43,66].

Fig. 5(b) illustrates the decomposition of H_2O_2 during CWPO of PCM runs and shows that CoFe nanocatalyst leads to the slowest degradation of the H_2O_2. However, different decomposition profiles were found for reactions involving the hybrid multi-core shell magnetic nanocatalysts, CoFe@C_{PG} and CoFe@C_{RF}, since those materials led to values of H_2O_2 decomposition of 52% and 100% after 6 h of reaction, respectively. Their unique behavior in the degradation of H_2O_2 helps to explain their behavior in the removal of PCM, with CoFe@C_{RF} also removing PCM faster than CoFe@C_{PG} does. The higher activity of CoFe@C_{RF} can be ascribed to its high surface area (Table 1), as increasing the surface area results in an increase in the number of active sites that can donate electrons for the decomposition of H_2O_2 into the desired radicals [38, 65]. Thus, the order of activity of the nanocatalyst in both H_2O_2 decomposition and PCM abatement is as follows: CoFe@C_{RF} > CoFe@C_{PG} > CoFe. The capacity of the catalysts to decompose H_2O_2 in absence of PCM was also evaluated, and the results are discussed in Text S5 and Fig. S11.

This more efficient decomposition of H_2O_2 in the presence of CoFe@C_{PG} is reflected in the degradation of molecules containing aromatic rings, ARM (Fig. S12). In the presence of CoFe@C_{PG}, it is possible to observe a higher concentration of ARM in the first 15 min of reaction,

Table 1
Physico-chemical characterization of matrices used for the CWPO of PCM.

	Bottle	River	Hospital	UP
TOC (mg L^{-1})	6.9 ± 0.3	35.0 ± 1.4	26.8 ± 1.1	2.6 ± 0.2
pH	7.6 ± 0.1	8.1 ± 0.2	5.9 ± 0.1	7.0 ± 0.1
Conductivity (μS cm^{-1})	83.8 ± 1.4	187.9 ± 2.6	683.0 ± 3.3	1.2 ± 0.2
Chloride (mg L^{-1})	17.72 ± 0.3	8.86 ± 0.2	121.42 ± 0.4	< 0.01.
Iron (mg L^{-1})	0.8 ± 0.1	8. 8 ± 0.1	4.6 ± 0.1	< 0.01
ARM (mg_{PCM} L^{-1})	0.4 ± 0.0	1.4 ± 0.0	6.6 ± 0.0	< 0.01
TN (mg L^{-1})	1.1 ± 0.05	4.6 ± 0.2	42.7 ± 1.8	< 0.01

followed by a constant decrease up to 24 h, when approximately 90% of the ARM compounds are removed. In the presence of CoFe@C_{RF} and CoFe, the ARM removals attained were only 60% and 55%, respectively. Although the HPLC method was calibrated to identify and quantify many of the expected oxidized intermediates products of PCM (*p*-nitrocatechol, hydroquinone, *p*-nitrophenol, resorcinol, *p*-benzoquinone, pyrocatechol, trans-muconic acid, and phenol [67]), none of them were identified through the samples taken from reaction media during all the CWPO experiments. Instead, only one peak (in addition to the PCM chromatogram peak) was observed in all chromatograms at 13.4 min of retaining time employing the HPLC method. Although the identification of the peak was not possible, it was monitored during all CWPO assays. The profile of the peak area upon reaction time detected in HPLC is represented in Fig. S13. Similarly, as observed for ARM compounds, in the presence of CoFe@C_{PG}, the oxidized intermediate detected in HPLC has a sharp increase in the first 30 min of reaction, followed by a sharp decrease, and after 8 h of reaction, it can no longer be detected. In the presence of CoFe, the maximum concentration is achieved at 4 h of reaction and the peak is no longer detected only after 24 h of reaction. For CoFe@C_{RF}, the behavior in the first 1 h of reaction is similar to PG-coated material, with a sharp increase of this intermediate in 30 min of reaction. However, from 1 h of reaction onwards, the intermediate slowly decreases up to 6 h of reaction, and remains in the reaction medium up to the end. The accumulation of this intermediate molecule is likely due to the fast decomposition of H_2O_2 in the presence of CoFe@C_{RF}: with no more H_2O_2 after 15 min of reaction (Fig. 5(b)), there is no H_2O_2 available for generating hydroxyls and oxidize the intermediate. Both CoFe and CoFe@C_{PG} allowed the complete decomposition of the intermediate because there was still H_2O_2 available for the reaction.

The adsorption of PCM was assessed at the same operating conditions as those used in CWPO of PCM but without the use of H_2O_2. At those operating conditions, CoFe@C_{RF} removed the highest amount of PCM (23%), followed by CoFe@C_{PG} (7%) and CoFe (4%) after 6 h of contact time (Fig. S14). The adsorption of PCM is closely related to the surface area of each nanoparticle, with a regression coefficient of $R^2 = 0.986$ (Fig. S15). As a result, its increased adsorption can likewise be connected with PCM's fast removal in the presence of CoFe@C_{RF} during CWPO runs. If the $d_{removal}$ (calculated according to Eq. (S2)) is the parameter considered, it is possible to observe that CoFe@C_{PG} activity surpasses that of CoFe@C_{RF} from 4 h of reaction onwards, indicating that oxidation plays a more significant role than adsorption (Fig. S16).

The TOC abatement obtained during the CWPO of PCM experiments for each nanocatalyst and blank run (without catalyst) is shown in Fig. S17. The TOC removal observed for all nanocatalysts overcame the non-catalytic run by up to 55%. The highest TOC removal was obtained for CoFe@C_{RF} (65%), closely followed by CoFe@C_{PG} (63%). The TOC removal in the presence of CoFe was the lowest one observed (40%). Despite the higher TOC removal observed for the nanocatalyst prepared in traditional coating procedure, the efficiency of H_2O_2 consumption (η_{H2O2}, determined as TOC and H_2O_2 conversions ratio according to Eq. (S3) [68]) is higher for CoFe@C_{PG}, reaching around 90% as shown in Fig. S17 (8 h of reaction time). The efficiency in the consumption of H_2O_2 observed for this study was higher than that reported in other works dealing with pollutant removal by similar processes using H_2O_2 [45,56,68]. Fig. 6 brings an overview of the screening parameters considered during the discussion of the present section. It is easily observed that CoFe@C_{PG} outperforms the other two catalysts in almost all parameters taken into consideration, and thus, it was chosen for further studies.

The stability of all the catalysts and the recyclability of the best catalyst (CoFe@C_{PG}) were assessed, and the results are discussed in Text S6 and Fig. S18-21.

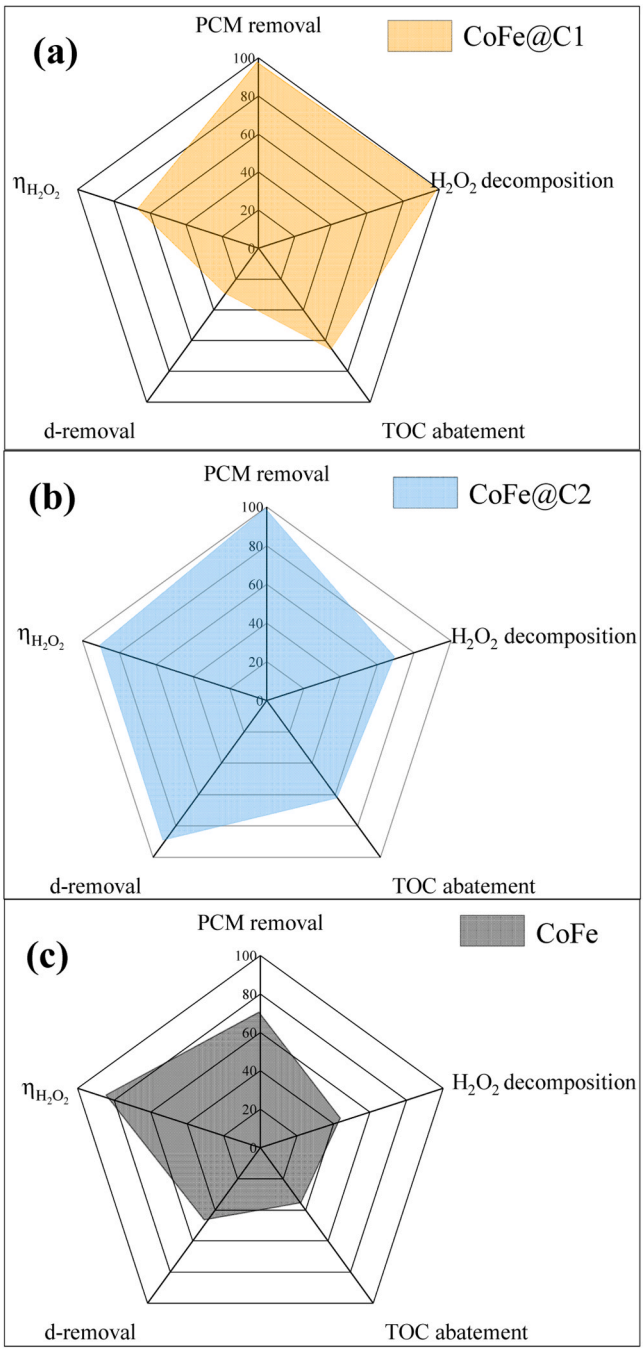

Fig. 6. Comparison between the performance of (a) CoFe@C_{RF}, (b) CoFe@C_{PG}, and (c) CoFe in screening PCM oxidation runs. PCM removal, TOC abatement, $d_{removal}$, and H_2O_2 decomposition are represented after 8 h and H_2O_2 consumption efficiency (η_{H2O2}) was calculated at 8 h of reaction. $d_{removal}$ was calculated according to Eq. (S2), and η_{H2O2} was determined according to Eq. (S3).

3.6. Catalytic wet peroxide oxidation of paracetamol: effect of distinct aqueous matrices

The result obtained for the physico-chemical characterization of the liquid mediums used for the reactions is shown in Table 1. Compared to the ultrapure matrix used for screening the catalysts, the composition of the chosen matrices is challenging, especially considering the presence of chloride anions known to act as scavenging radicals in Fenton-like reactions [26,69]. The measurement of bicarbonate anions was not considered here because previous studies have reported that this radical

has no significant scavenging effect when the pH is below 6.35 [70]. The TOC value for bottled water exceeds the maximum level for relatively clean waters (3 mg L^{-1}), which is not necessarily a standard value for drinking water [71]. The Total Organic Carbon (TOC) value of the hospital wastewater is below the values reported in the literature for other residues from comparable sources, ranging from 64.9 to 260.3 mg L^{-1} [72,73]. Nevertheless, it is crucial to emphasize that actual wastewaters exhibit significant seasonal variations in composition, greatly impacting the characterization of real matrices. However, it should be noted that this study does not specifically focus on this aspect. The main parameter influencing the TOC value for river waters is related to the urbanization rate close to the region where the collection occurred. For this reason, the value found for this study agrees with the literature since the collection region is urbanized [74].

The results obtained for the CWPO of PCM in a distinct aqueous medium using the same operating conditions as those employed in ultrapure water (adjusted pH to 3.5 with 0.5 M H_2SO_4, 80 ºC and equal concentration of PCM, H_2O_2 and catalyst) are shown in Fig. 7. The non-catalytic (N.C.) run revealed an H_2O_2 decomposition higher than observed in previous reactions performed using ultrapure water (10%) as a matrix for bottled water (49.4%), hospital wastewater (41.5%), and river water (47.3%). These results are related to the thermal decomposition of H_2O_2 and the higher amount of iron inherently present in liquid media (0.8, 8. 8 and 4.6 mg L^{-1} for bottle, Fervença river and hospital aqueous matrices), allowing for a contribution of homogeneous Fenton reaction. As previously stated, the highest PCM removal obtained for non-catalytic runs in real wastewater *vs.* ultrapure matrix is related to

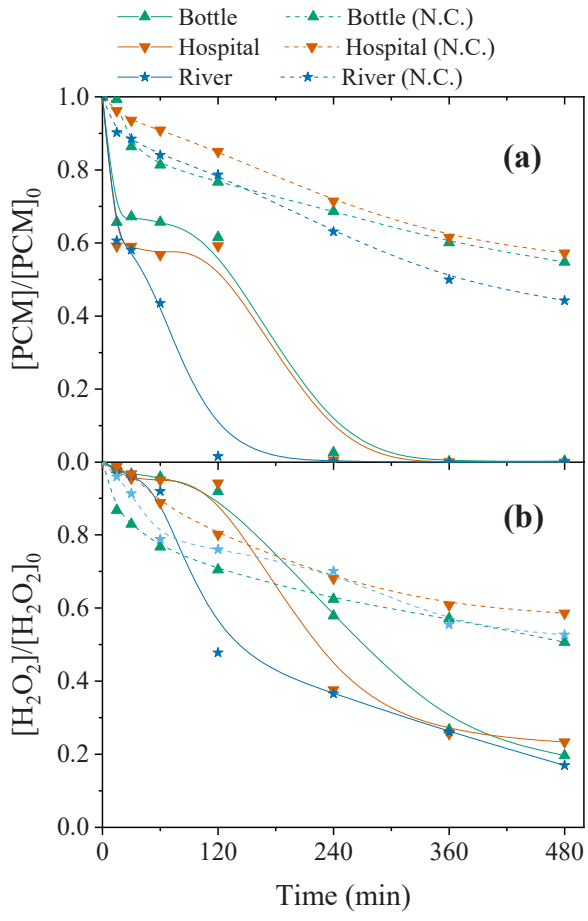

Fig. 7. Normalized concentration of (a) PCM and (b) H_2O_2 upon reaction time in CWPO reactions carried out using different liquid matrices with CoFe@C_{PG} catalyst and without catalyst (N.C.). Operating conditions: $[PCM]_0$ = 100 mg L^{-1}, $[H_2O_2]_0$ = 474 mg L^{-1}, [catalyst] = 2.5 g L^{-1}, pH_0 = 3.5, T = 80 °C.

the formation of hydroxyl radicals. Nonetheless, all catalytic runs overcome the non-catalytic run by at least 44% regarding PCM removal and 31% for H_2O_2 decomposition after 8 h of reaction. The PCM removal profile in catalytic runs for hospital and bottled waters had a slightly different tendency in different matrices compared to the screening run performed with ultrapure water as a matrix. The difference is related to the composition of the matrices used here, comprised of chloride ions that slow the reaction rate. Despite the increased complexity of the matrices, all PCM was removed from the reaction medium after 6 h of reaction, which is the same result observed for the run performed in ultrapure water. Interestingly, the PCM removal profile obtained for the river water matrix revealed a higher PCM removal rate than ultrapure water. This occurs due to the iron in river water and the low amount of chloride ions in this matrix. By this means, the iron in the river water contributes to the removal of PCM by converting more hydroxyl radicals without being hindered by scavengers.

Regarding H_2O_2 decomposition into hydroxyl radicals shown in Fig. 7(b), the profile observed with the three matrices differed from that observed in the screening test. The decomposition profile obtained using ultrapure water as a matrix revealed higher decomposition of H_2O_2 in the first 2 h of the reaction than observed here. For instance, around 52.3% of H_2O_2 was decomposed in the ultrapure water, while 8.1%, 5.8%, and 63.4% were decomposed in bottled, hospital, and river matrices after 2 h of reaction. The lowest decomposition of H_2O_2 obtained agrees with the difference in PCM removal observed for bottled and hospital waters reactions. For the river water, the effect mentioned above is proven by the highest decomposition of H_2O_2 observed after 2 h of reaction. Despite the delayed H_2O_2 decomposition reported for the bottled and hospital waters, the catalyst allows decomposing about 80.6% and 76.6% of H_2O_2 after 8 h of reaction, respectively, which is higher than the result obtained in ultrapure water (70.5%). For the reaction carried out using river waters, the H_2O_2 decomposition reached 83.0%, which is also more than observed for ultrapure water.

The results obtained for ARM during the reaction are shown in Fig. S22 in terms of PCM equivalent. The response exhibited in the graph was measured by discounting the PCM contribution based on HPLC results. The initial concentration observed for all matrices is related to the presence of other aromatic compounds rather than paracetamol and intermediates. An increase in aromatic compound response can be observed during the reaction, reaching an equivalent concentration of almost 500 mg_{PCM} L^{-1}. It is important to highlight that different chemical aromatic species have different sensibilities for this analysis, which is why the results reached high equivalent concentrations of PCM. For all reactions, the aromatic response increased in the first 2 h, decreasing to less than the initial values at the end of the reaction. The fact that equivalent aromatic concentrations reached lower values than initially measured is related to the oxidation of aromatic compounds naturally occurring in the matrices beyond the oxidation of the generated aromatic intermediates during PCM degradation. For instance, equivalent aromatic concentrations went from 119.0, 182.1, and 41.5 mg_{PCM} L^{-1} to 12.7, 25.9, and 10.4 mg_{PCM} L^{-1} in bottled, hospital wastewater, and river water, representing removals of 89%, 86%, and 75%, respectively, of aromatic-containing compounds from the matrices.

The results obtained by TOC removal after 8 h of reaction for non-catalytic and catalytic runs are expressed in Fig. S23, along with the consumption efficiency of H_2O_2 (η_{H2O2}). The results show that the non-catalytic run for bottled and hospital water removed about 15.3% and 14.5% of TOC, respectively, whereas the removal reached 22.3% in river water. The higher removal observed for river water is related to the higher H_2O_2 decomposition obtained for this matrix. Nonetheless, catalytic runs could overcome the results obtained without a catalyst for all cases, degrading 40.4%, 37.2%, and 29.1% more organic matter than non-catalytic runs for bottled, hospital, and river waters. The efficiency of H_2O_2 consumption was about the same for all matrices (60–70%), with a slightly higher value for the reaction carried out using bottled water as a matrix. The lower η_{H2O2} compared to the run conducted in

ultrapure water may be ascribed to the distinct profile of H_2O_2 decomposition due to a contribution of homogeneous Fenton from iron ions in the matrices, resulting in less TOC being removed. The final value obtained for TOC abatement in different matrices, 32.1, 49.6, and 43.2 mg L^{-1}, is greater than TOC value in pure matrices. However, the TOC abatement is likely influenced by the removal of other organic pollutants present in the matrices since organic pollutant degradation by hydroxyl radical is a non-selective reaction [75]. It is important to highlight that this effect is not visual using TOC results because the final reaction byproducts are carboxylic acids [76], which are refractory to CWPO and contribute to TOC count.

4. Conclusions

The innovative method proposed for synthesizing a thin-layered carbon shell for protecting an active metal core for CWPO reactions has been successfully achieved. The synthesized novel nanocatalyst has displayed a higher catalytic activity compared to the one coated with resorcinol/formaldehyde resin. In addition, the multi-core shell magnetic nanocatalyst prepared by phloroglucinol and glyoxal resin (CoFe@C_{PG}) shows higher stability, as demonstrated by the negligible iron leaching observed in the CWPO reaction with CoFe@C_{PG}. The high stability of the material allowed its reutilization in 3 cycles, resulting in similar removals of PCM and TOC. The catalyst was also applied in CWPO runs considering real water matrices, and the results obtained were consistent with those obtained under a simulated matrix. This highlights the robustness of the catalyst for real-world applications. For instance, the catalyst design considered here could be used to prepare other materials changing the core to evaluate the efficiency in similar reactions. Additionally, the result obtained for experiments in real matrices has proven the feasibility of utilizing hybrid catalysts to remove organic pollutants by catalytic wet peroxide oxidation. We anticipate that catalysts prepared *via* both methodologies used here could achieve performances as high as reported in this study considering other organic pollutants and similar reaction conditions.

Furthermore, characterizing the intermediate particles (CoFe@R_x and CoFe@SiO_2. C_x) allows a better understanding of the role of each step in the synthesis, permitting a more rational decision in the design of new catalysts.

In brief, highly active, stable, and versatile nanocatalysts can be prepared for advanced oxidation processes by carbon coating with phloroglucinol and glyoxal resin and thermal treatment since it was demonstrated that the nanocatalyst developed in this study does not show metal leaching, can be used in successive runs with no loss of catalytic activity and show high performance in the removal of micropollutants from different real matrixes.

CRediT authorship contribution statement

Adriano S. Silva: Conceptualization, Investigation, Formal analysis, Methodology, Visualization, Writing – original draft. **Arnaldo V. Dias**: Investigation, Formal analysis. **Fernanda F. Roman**: Investigation, Formal analysis, Writing – original draft. **Jose L. Diaz de Tuesta**: Writing – review & editing, Conceptualization, Methodology, Funding acquisition, Supervision. **Ana P. Ferreira da Silva**: Writing – review & editing. **Manuel Bañobre-López**: Investigation, Writing – review & editing. **Francis Deepak**: Investigation, Writing – review & editing. **Ana M. C Ferrari:** Writing – review & editing, Supervision. **Helder T. Gomes**: Funding acquisition, Project administration, Writing – review & editing, Supervision.

Declaration of Competing Interest

The authors declare that they have no known competing financial interests or personal relationships that could have appeared to influence the work reported in this paper.

Data availability

Data will be made available on request.

Acknowledgments

This work was financially supported by project RTChip4Theranostics (NORTE-01–0145-FEDER-029394), by CIMO (UIDB/00690/2020) through FEDER under Program PT2020. Fernanda F. Roman acknowledges the Foundation for Science and Technology (FCT) and the European Social Fund (FSE) for the individual research grant with reference SFRH/BD/143224/2019. Adriano Silva and Ana Paula F. da Silva were supported by the doctoral Grant SFRH/BD/151346/2021 and PRT/BD/153090/2021 financed by the Portuguese Foundation for Science and Technology (FCT) with funds from NORTE2020, under MIT Portugal Program. Jose L. Diaz De Tuesta acknowledges the financial support through the program of Atracción al Talento of Comunidad de Madrid (Spain) for the individual research grant 2022-T1/AMB-23946.

Appendix A. Supporting information

Supplementary data associated with this article can be found in the online version at doi:10.1016/j.jece.2023.110806.

References

[1] L. Rizzo, et al., Sci. Total Environ. vol. 655 (2019) 986–1008, https://doi.org/10.1016/j.scitotenv.2018.11.265.
[2] Q.H. Zhang, et al., Environ. Int. vol. 92–93 (2016) 11–22, https://doi.org/10.1016/j.envint.2016.03.024.
[3] D. Yadav, et al., Chemosphere vol. 272 (2021), 129492, https://doi.org/10.1016/j.chemosphere.2020.129492.
[4] J. Ryu, J. Oh, S.A. Snyder, Y. Yoon, Environ. Monit. Assess. vol. 186 (5) (2014) 3239–3251, https://doi.org/10.1007/s10661-013-3613-5.
[5] Y. Luo, et al., Sci. Total Environ. vol. 473–474 (2014) 619–641, https://doi.org/10.1016/j.scitotenv.2013.12.065.
[6] M. D'Alessio, S. Onanong, D.D. Snow, C. Ray, Sci. Total Environ. vol. 631–632 (2018) (2018) 1360–1370, https://doi.org/10.1016/j.scitotenv.2018.03.100.
[7] L. Joseph, et al., Chem. Eng. J. vol. 369 (2019) 928–946, https://doi.org/10.1016/j.cej.2019.03.173.
[8] S. Kim, et al., no. November 2017, Chem. Eng. J. vol. 335 (2018) 896–914, https://doi.org/10.1016/j.cej.2017.11.044.
[9] S. Khan, M. Naushad, M. Govarthanan, J. Iqbal, S.M. Alfadul, Environ. Res. vol. 207 (2022), 112609, https://doi.org/10.1016/j.envres.2021.112609.
[10] M. Bilal, M. Adeel, T. Rasheed, Y. Zhao, H.M.N. Iqbal, no. October 2018, Environ. Int. vol. 124 (2019) 336–353, https://doi.org/10.1016/j.envint.2019.01.011.
[11] L. Li, et al., J. Clean. Prod. vol. 210 (2019) 1324–1342, https://doi.org/10.1016/j.jclepro.2018.11.087.
[12] S.P.M. Menacherry, U.K. Aravind, C.T. Aravindakumar, J. Environ. Chem. Eng. vol. 10 (4) (2022), 108155, https://doi.org/10.1016/j.jece.2022.108155.
[13] M.J. Benotti, R.A. Trenholm, B.J. Vanderford, J.C. Holady, B.D. Stanford, S. A. Snyder, Environ. Sci. Technol. vol. 43 (3) (2009) 597–603, https://doi.org/10.1021/es801845a.
[14] M. Priyadarshini, I. Das, M.M. Ghangrekar, L. Blaney, J. Environ. Manag. vol. 316 (May) (2022), 115295, https://doi.org/10.1016/j.jenvman.2022.115295.
[15] A.L. Spongberg, J.D. Witter, Sci. Total Environ. vol. 397 (1–3) (2008) 148–157, https://doi.org/10.1016/j.scitotenv.2008.02.042.
[16] N. Liu, et al., Chemosphere vol. 207 (8) (2018) 682–689, https://doi.org/10.1016/j.chemosphere.2018.05.093.
[17] M. Naushad, G. Sharma, Z.A. Alothman, J. Clean. Prod. vol. 241 (2019), 118263, https://doi.org/10.1016/j.jclepro.2019.118263.
[18] N.H. Tran, J. Li, J. Hu, S.L. Ong, Environ. Sci. Pollut. Res. vol. 21 (6) (2014) 4727–4740, https://doi.org/10.1007/s11356-013-2428-9.
[19] S. Chowdhury, R. Balasubramanian, Adv. Colloid Interface Sci. vol. 204 (2014) 35–56, https://doi.org/10.1016/j.cis.2013.12.005.
[20] B. Corzo, T. de la Torre, C. Sans, E. Ferrero, J.J. Malfeito, Chem. Eng. J. vol. 326 (2017) 1–8, https://doi.org/10.1016/j.cej.2017.05.108.
[21] Á. Soriano, D. Gorri, A. Urtiaga, Water Res vol. 112 (2017) 147–156, https://doi.org/10.1016/j.watres.2017.01.043.
[22] J.L. Acero, F. Javier Benitez, F.J. Real, F. Teva, Chem. Eng. J. vol. 210 (2012) 1–8, https://doi.org/10.1016/j.cej.2012.08.043.
[23] B.G. Kwon, H.J. Lim, S.H. Na, B.I. Choi, D.S. Shin, S.Y. Chung, Chemosphere vol. 109 (2014) 221–225, https://doi.org/10.1016/j.chemosphere.2014.01.072.
[24] A.S. Silva, M. Seitovna Kalmakhanova, B. Kabykenovna Massalimova, J.G. Sgorlon, J.L. Diaz de Tuesta, H. Gomes (Aug), Catalysts (2019), https://doi.org/10.3390/catal9090705.
[25] J.L. Diaz De Tuesta, et al., J. Environ. Chem. Eng. vol. 9 (1) (2021), 105004, https://doi.org/10.1016/j.jece.2020.105004.

[26] G. de Freitas Batista, F.F. Roman, J.L.D. de Tuesta, R.V. Mambrini, P. Praça, H. T. Gomes, Catalysts vol. 12 (2) (2022), https://doi.org/10.3390/catal12020238.
[27] J.L. Diaz, de Tuesta et al. (Apr), Catal. Today (2023), 114162, https://doi.org/10.1016/j.cattod.2023.114162.
[28] R. Dewil, D. Mantzavinos, I. Poulios, M.A. Rodrigo, J. Environ. Manag. vol. 195 (2017) 93–99, https://doi.org/10.1016/j.jenvman.2017.04.010.
[29] J. Wang, R. Zhuan, Sci. Total Environ. vol. 701 (2020), 135023, https://doi.org/10.1016/j.scitotenv.2019.135023.
[30] B.A. Wols, C.H.M. Hofman-Caris, Water Res vol. 46 (9) (2012) 2815–2827, https://doi.org/10.1016/j.watres.2012.03.036.
[31] Y. Liu, J. Wang, J. Hazard. Mater. vol. 250–251 (2013) 99–105, https://doi.org/10.1016/j.jhazmat.2013.01.050.
[32] M. Gągol, A. Przyjazny, G. Boczkaj, no. November 2017, Chem. Eng. J. vol. 338 (2018) 599–627, https://doi.org/10.1016/j.cej.2018.01.049.
[33] P. Chanikya, P.V. Nidheesh, D. Syam Babu, A. Gopinath, M. Suresh Kumar, no. May 2020, Sep. Purif. Technol. vol. 254 (2021), 117570, https://doi.org/10.1016/j.seppur.2020.117570.
[34] V. Kumar, M.P. Shah, in: E.T.P. Shah (Ed.), M. P. B. T.-A. O. P. for, Elsevier, 2021, pp. 1–31, https://doi.org/10.1016/B978-0-12-821011-6.00001-3.
[35] J.L. Diaz de Tuesta, A. Quintanilla, J.A. Casas, J.J. Rodriguez, Appl. Catal. B Environ. vol. 209 (2017) 701–710, https://doi.org/10.1016/j.apcatb.2017.03.031.
[36] J.L. Diaz de Tuesta, et al., no. August 2019, Catal. Today vol. 356 (2020) 216–225, https://doi.org/10.1016/j.cattod.2019.08.033.
[37] F.F. Roman, J.L. Diaz De Tuesta, P. Praça, A.M.T. Silva, J.L. Faria, H.T. Gomes, J. Environ. Chem. Eng. vol. 9 (1) (2021) 1–9, https://doi.org/10.1016/j.jece.2020.104888.
[38] R.S. Ribeiro, et al., Appl. Catal. B Environ. vol. 219 (2017) 645–657, https://doi.org/10.1016/j.apcatb.2017.08.013.
[39] R.P. Rocha, M.F.R. Pereira, J.L. Figueiredo, no. April 2019, Catal. Today vol. 356 (2020) 189–196, https://doi.org/10.1016/j.cattod.2019.04.047.
[40] M. Martin-Martinez, et al., no. October 2018, Catal. Today vol. 357 (2020) 332–340, https://doi.org/10.1016/j.cattod.2019.03.014.
[41] R.S. Ribeiro, A.M.T. Silva, L.M. Pastrana-Martínez, J.L. Figueiredo, J.L. Faria, H. T. Gomes, Catal. Today vol. 249 (2015) 204–212, https://doi.org/10.1016/j.cattod.2014.10.004.
[42] M. Pacheco-Álvarez, R. Picos Benítez, O.M. Rodríguez-Narváez, E. Brillas, J. M. Peralta-Hernández, Chemosphere vol. 303 (March) (2022), https://doi.org/10.1016/j.chemosphere.2022.134883.
[43] R.S. Ribeiro, A.M.T. Silva, P.B. Tavares, J.L. Figueiredo, J.L. Faria, H.T. Gomes, Catal. Today vol. 280 (2017) 184–191, https://doi.org/10.1016/j.cattod.2016.04.040.
[44] R.S. Ribeiro, A.M.T. Silva, P.B. Tavares, J.L. Figueiredo, J.L. Faria, H.T. Gomes, Catal. Today vol. 280 (. 2017) 184–191, https://doi.org/10.1016/j.cattod.2016.04.040.
[45] N.M.C. Guari, A.S. Silva, J.L. Diaz de Tuesta, W.E. Pottker, P.Y. Cordeiro, and H.T. Gomes, 2022, doi: https://doi.org/10.30955/gnj.004309.
[46] R.S. Ribeiro, J. Gallo, M. Bañobre-López, A.M.T. Silva, J.L. Faria, H.T. Gomes, Chem. Eng. J. vol. 376 (2019) (2019), 120012, https://doi.org/10.1016/j.cej.2018.09.173.
[47] S. Duhayon, P. Hoet, G. Maele-Fabry, D. Lison, Int. Arch. Occup. Environ. Health vol. 81 (6) (2008) 695–710, https://doi.org/10.1007/s00420-007-0241-9.
[48] R.T. Mayes, C. Tsouris, J.O. Kiggans, S.M. Mahurin, D.W. Depaoli, S. Dai, J. Mater. Chem. vol. 20 (39) (2010) 8674–8678, https://doi.org/10.1039/c0jm01911a.
[49] S. Kralj, T. Potrc, P. Kocbek, S. Marchesan, D. Makovec, Curr. Med. Chem. vol. 24 (5) (2017) 454–469.
[50] A.S. Silva, L. Diaz, S. Berberich, F.L. Deepak, M. Bañobre-lópez, Nanoscale (2022) 7220–7232, https://doi.org/10.1039/d1nr08550f.
[51] M. Sopronyi, F. Sima, C. Vaulot, L. Delmotte, A. Bahouka, C.M. Ghimbeu, Sci. Rep. vol. 6 (December) (2016) 1–13, https://doi.org/10.1038/srep39617.
[52] J.L. Diaz De Tuesta, et al., J. Environ. Chem. Eng. vol. 10 (5) (2022), https://doi.org/10.1016/j.jece.2022.108143.
[53] M. Houshiar, F. Zebhi, Z.J. Razi, A. Alidoust, Z. Askari, J. Magn. Magn. Mater. vol. 371 (2014) 43–48, https://doi.org/10.1016/j.jmmm.2014.06.059.
[54] M. Sajjia, M. Oubaha, M. Hasanuzzaman, A.G. Olabi, Ceram. Int, PART A vol. 40 (1) (2014) 1147–1154, https://doi.org/10.1016/j.ceramint.2013.06.116.
[55] S. Xavier, S. Thankachan, B.P. Jacob, E.M. Mohammed, Nanosyst. Phys., Chem. Math. vol. 4 (3) (2013) 430–437.
[56] A.S. Silva, M.S. Kalmakhanova, B.K. Massalimova, J.L.D. de Tuesta, H.T. Gomes, Catalysts vol. 9 (2019) 705, https://doi.org/10.3390/catal9090705.
[57] Z. Liu, Q. Shen, C. Zhou, L. Fang, M. Yang, T. Xia, Catalysts vol. 8 (10) (2018), https://doi.org/10.3390/catal8100445.
[58] M. Shi, et al., J. Alloy. Compd. vol. 512 (1) (2012) 165–170, https://doi.org/10.1016/j.jallcom.2011.09.057.
[59] E.P. Muniz, et al., J. Clean. Prod. vol. 265 (2020), https://doi.org/10.1016/j.jclepro.2020.121712.
[60] J. Venturini, R.Y.S. Zampiva, S. Arcaro, C.P. Bergmann, Ceram. Int. vol. 44 (11) (2018) 12381–12388, https://doi.org/10.1016/j.ceramint.2018.04.026.
[61] M. Abbas, et al., Ceram. Int. vol. 40 (2) (2014) 3269–3276, https://doi.org/10.1016/j.ceramint.2013.09.109.
[62] A.S. Ponce, E.F. Chagas, R.J. Prado, C.H.M. Fernandes, A.J. Terezo, E. Baggio-Saitovitch, J. Magn. Magn. Mater. vol. 344 (2013) 182–187, https://doi.org/10.1016/j.jmmm.2013.05.056.
[63] D. Tomar, P. Jeevanandam, J. Alloy. Compd. vol. 843 (2020), 155815, https://doi.org/10.1016/j.jallcom.2020.155815.
[64] S. Ouaissa, A. Benyoussef, G.S. Abo, M. Ouaissa, M. Hafid, Phys. Procedia vol. 75 (2015) 792–801, https://doi.org/10.1016/j.phpro.2015.12.103.
[65] R.S. Ribeiro, A.M.T. Silva, J.L. Figueiredo, J.L. Faria, H.T. Gomes, Appl. Catal. B Environ. vol. 187 (2016) 428–460, https://doi.org/10.1016/j.apcatb.2016.01.033.
[66] R. Zhu, et al., Appl. Catal. B Environ. vol. 270 (March) (2020), 118891, https://doi.org/10.1016/j.apcatb.2020.118891.
[67] E. Leyva, E. Moctezuma, K.M. Baines, S. Noriega, E. Zarazua, Curr. Org. Chem. vol. 22 (1) (2017) 2–17, https://doi.org/10.2174/1385272821666171019145520.
[68] F.F. Roman, et al., *Catal. Today* (2023) 2022, https://doi.org/10.1016/j.cattod.2023.01.008.
[69] R.S. Ribeiro, et al., no. September 2021, J. Environ. Manag. vol. 308 (2022), 114622, https://doi.org/10.1016/j.jenvman.2022.114622.
[70] S.A. Mirzaee, N. Jaafarzadeh, H.T. Gomes, S. Jorfi, M. Ahmadi, Chem. Eng. J. vol. 370 (March) (2019) 372–386, https://doi.org/10.1016/j.cej.2019.03.202.
[71] A. Ikem, S. Odueyungbo, N.O. Egiebor, K. Nyavor, Sci. Total Environ. vol. 285 (1–3) (2002) 165–175, https://doi.org/10.1016/S0048-9697(01)00915-9.
[72] S. Veli, A. Arslan, D. Bingöl, Clean. - Soil, Air, Water vol. 44 (11) (2016) 1516–1522, https://doi.org/10.1002/clen.201500729.
[73] S. Top, M. Akgün, E. Kıpçak, M.S. Bilgili, Water Res vol. 185 (2020), 116279, https://doi.org/10.1016/j.watres.2020.116279.
[74] Y. Huang, L. Zhang, L. Ran, Water (Switz.) vol. 14 (13) (2022), https://doi.org/10.3390/w14132102.
[75] Y. Zhu, R. Zhu, Y. Xi, J. Zhu, G. Zhu, H. He, Appl. Catal. B Environ. vol. 255 (May) (2019), 117739, https://doi.org/10.1016/j.apcatb.2019.05.041.
[76] J.L. Diaz de Tuesta, A. Quintanilla, D. Moreno, V.R. Ferro, J.A. Casas, Catalysts vol. 10 (5) (2020), https://doi.org/10.3390/catal10050548.